Determining the band gap and mean kinetic energy of atoms from reflection electron energy loss spectra

M. Vos, G. G. Marmitt, Y. Finkelstein, and R. Moreh

Citation: The Journal of Chemical Physics **143**, 104203 (2015); doi: 10.1063/1.4929911
View online: http://dx.doi.org/10.1063/1.4929911
View Table of Contents: http://scitation.aip.org/content/aip/journal/jcp/143/10?ver=pdfcov
Published by the AIP Publishing

Articles you may be interested in

Band gap and defect states of MgO thin films investigated using reflection electron energy loss spectroscopy
AIP Advances **5**, 077167 (2015); 10.1063/1.4927547

Direct band gap measurement of Cu(In,Ga)(Se,S)2 thin films using high-resolution reflection electron energy loss spectroscopy
Appl. Phys. Lett. **106**, 261601 (2015); 10.1063/1.4923201

A reverse Monte Carlo method for deriving optical constants of solids from reflection electron energy-loss spectroscopy spectra
J. Appl. Phys. **113**, 214303 (2013); 10.1063/1.4809544

Detection of defect states in low-k dielectrics using reflection electron energy loss spectroscopy
J. Appl. Phys. **113**, 044109 (2013); 10.1063/1.4788980

Measurement of optical constants of Si and SiO 2 from reflection electron energy loss spectra using factor analysis method
J. Appl. Phys. **107**, 083709 (2010); 10.1063/1.3346345

This article is copyrighted as indicated in the article. Reuse of AIP content is subject to the terms at: http://scitation.aip.org/termsconditions. Downloaded to IP: 130.56.107.4 On: Mon, 02 Nov 2015 03:18:08

Determining the band gap and mean kinetic energy of atoms from reflection electron energy loss spectra

M. Vos,[1] G. G. Marmitt,[1,2] Y. Finkelstein,[3] and R. Moreh[4]
[1]*Atomic and Molecular Physics Laboratories, Research School of Physics and Engineering, Australian National University, Canberra ACT, Australia*
[2]*Instituto de Fisica da Universidade Federal do Rio Grande do Sul, Avenida Bento Goncalves 9500, 91501-970 Porto Alegre, RS, Brazil*
[3]*Nuclear Research Center — Negev, Beer-Sheva 84190, Israel*
[4]*Physics Department, Ben-Gurion University of the Negev, Beer-Sheva 84105, Israel*

(Received 12 July 2015; accepted 20 August 2015; published online 9 September 2015)

Reflection electron energy loss spectra from some insulating materials ($CaCO_3$, Li_2CO_3, and SiO_2) taken at relatively high incoming electron energies (5–40 keV) are analyzed. Here, one is bulk sensitive and a well-defined onset of inelastic excitations is observed from which one can infer the value of the band gap. An estimate of the band gap was obtained by fitting the spectra with a procedure that includes the recoil shift and recoil broadening affecting these measurements. The width of the elastic peak is directly connected to the mean kinetic energy of the atom in the material (Doppler broadening). The experimentally obtained mean kinetic energies of the O, C, Li, Ca, and Si atoms are compared with the calculated ones, and good agreement is found, especially if the effect of multiple scattering is taken into account. It is demonstrated experimentally that the onset of the inelastic excitation is also affected by Doppler broadening. Aided by this understanding, we can obtain a good fit of the elastic peak and the onset of inelastic excitations. For SiO_2, good agreement is obtained with the well-established value of the band gap (8.9 eV) only if it is assumed that the intensity near the edge scales as $(E - E_{gap})^{1.5}$. For $CaCO_3$, the band gap obtained here (7 eV) is about 1 eV larger than the previous experimental value, whereas the value for Li_2CO_3 (7.5 eV) is the first experimental estimate. © *2015 AIP Publishing LLC.* [http://dx.doi.org/10.1063/1.4929911]

I. INTRODUCTION

The band gap of materials determines many of their electrical properties. The band gap is also the property that is rather difficult to calculate based on density functional theory (DFT). For wide-gap insulators, (Reflection) electron energy loss spectroscopy ((R)EELS) is often used to determine its magnitude, but quantitative extraction of the band gap value is often difficult and frequently relies on extrapolating the straight line corresponding to the leading edge of the loss structure. See, e.g., Ref. 1 for some recent examples. This procedure is not very rigorous and the accuracy of the obtained result is hard to judge. For low incoming energies, interpretation is even more difficult due to the significant contributions to the measured spectrum of both intrinsic surface states and defects present at the surface.

Within electron microscopy, the extraction of the band gap from the experimental (transmission) electron energy loss data was set on a more solid footing by Rafferty and Brown.[2] They devised a fitting procedure within the framework of the Bethe theory[3] and extracted the band gap based on the theoretical shape for the onset of the energy loss spectrum. We will try here to investigate if this approach works also for REELS, at relatively high energies when the contribution of surface losses should be small, and the surface condition is less critical as one probes relatively deep in materials.

A complicating factor is that at higher energies the large-angle deflection of electrons implies the transfer of a measurable amount of energy to the scattering atom. This transferred energy depends on the mass and the velocity of the scattering atom. Thus, the shape of the elastic peak is not a simple Gaussian corresponding to the experimental resolution and an accurate determination of the band gap requires quantitative understanding of these effects. All electrons detected in a REELS experiment have scattered elastically from a target atom, and hence are affected by these recoil losses. Electrons that contribute to the elastic peak have created no inelastic excitations in the solid. The onset of the energy loss spectrum, used to extract the band gap values, is due to projectiles that have created a single electron-hole pair in the target.

At very large incoming energies, the elastic peak of an electron scattered from a light atom in the target may be the same as the energy of an electron that has scattered elastically from a heavy atom *and* created an electron-hole pair. Understanding these spectra requires thus a good description of both the elastic peak and the onset of the band gap. It is this description that is the topic of this paper. The elastic peak is fitted based on the composition of the sample and the mean kinetic energy of the atoms present. In fact, the spectroscopy described here is one of the very few methods that can measure the mean kinetic energies of atoms directly. Hence, we describe how the mean kinetic energy (an interesting quantity in itself) can be calculated in some detail to see if the interpretation used here is realistic. In practice, from the measurement at high incoming energies (40 keV), one determines the mean kinetic energy $K_e(X)$ of element X and these values are compared

 © 2015 AIP Publishing LLC

This article is copyrighted as indicated in the article. Reuse of AIP content is subject to the terms at: http://scitation.aip.org/termsconditions. Downloaded to IP: 130.56.107.4 On: Mon, 02 Nov 2015 03:18:08

to calculated ones. At somewhat lower energies (5 keV), one can then fit the onset of the inelastic losses based on these kinetic energies. In some cases (e.g., Li_2CO_3), one requires a combined fit of spectra taken at different energies to get a good estimate of both the kinetic energy and the band gap.

II. THEORETICAL BACKGROUND

A. Band gap measurement

In a REELS spectrum of an insulator, the elastic peak is followed by a region of essentially zero intensity up to a certain energy loss after which there is additional intensity due to inelastic excitations. When we neglect defect states and polaronic excitations, the onset of the loss spectrum corresponds to the band gap. However, the onset is convoluted by the experimental resolution (and Doppler broadening). The band gap value assigned to an energy loss spectrum depends then on the shape of the loss function assumed. As statistics is limited, deconvolution of the experimental resolution is usually not an option and one has to rely on a model. The most crude, but widely used method of interpreting such a spectrum, is by approximating the leading edge by a straight line and assigning the band gap to the energy where this straight line intersects the energy axis. Drawing this line is not unique and the statistical error involved in this procedure is hard to trace.

For determining the band gap, one has to know the shape of the onset of the loss function. The often used straight line approximation assumes that the loss function near the onset resembles $C(E - E_{gap})$, but this assumption is usually made implicitly. In the context of EELS experiments in a transmission electron microscope (TEM), Rafferty and Brown[2] argued that the shape of the onset should be close to $(E - E_{gap})^{0.5}$ for direct gap semiconductors and $(E - E_{gap})^{1.5}$ for indirect gap semiconductors. This approach has been discussed in other TEM-related publications, noticeably in the context of an apparent sample-thickness dependence of the band gap and complications due to presence of Cherenkov radiation[4,5] and the effect of numerical treatment of the data on the band gap obtained.[6]

Can one use the Rafferty and Brown approach in a REELS experiment? This is not a trivial question. It completely neglects surface excitations which have a major influence in low energy REELS experiments, but it could become a reasonable approximation for REELS experiments at multiple keV in a non-surface sensitive geometry as described here. Another important difference is that in a TEM-EELS experiment there is an aperture that limits the range of momentum transfer q of the detected electron, see, e.g., Ref. 4 how this can be used to study indirect transitions. In REELS, one relies on elastic scattering to deflect the detected electrons, which corresponds to the absence of a limiting aperture. So our aim will be slightly more modest. Rather than assuming that the intensity near the band gap is proportional to $(E - E_{gap})$ (as is done implicitly in the straight line approximation), we will fit our data with $(E - E_{gap})^{0.5}$ and $(E - E_{gap})^{1.5}$ and see how the resulting band gap varies. This will give a range of band gap values that are consistent with the data, and a more precise determination will only be possible if an *a priori* assumption of the shape can be justified based on theory. It would be even more helpful if theory could not only describe the shape of the onset, but also provide an estimate of its intensity relative to that of the elastic peak.

For the measurement of the band gap with high-energy electrons to work, one needs a good understanding of the recoil effects that affect REELS measurements. This will be discussed next.

B. Recoil effects in high-energy REELS measurements

In a large-angle scattering event, there is momentum transferred from the projectile electron to a target. It turns out that the transferred momentum $\mathbf{q}$ is absorbed by a single atom, and the energy transferred to this atom (mass M_i) can be calculated, assuming that this atom is free. This recoil energy E_r depends then on the momentum $\mathbf{p}$ of the target atom before the collision,[7]

$$E_r = \frac{q^2}{2M_i} + \frac{\mathbf{q}\cdot\mathbf{p}}{M_i}. \quad (1)$$

E_r is thus equal to the energy transfer to a stationary atom $(q^2/2M_i)$ plus a Doppler broadening term. This equation is very similar to the one describing (x-ray) Compton scattering, and hence these experiments, when measuring the width of the peak, are sometimes described as electron Compton scattering (ECS). First, we will neglect the influence of multiple scattering and the magnitude of $\mathbf{q}$ is then set by the incoming energy and the angle between the electron gun and the analyzer: θ_{scat}, which is 135° in our case. For isotropic targets (polycrystalline or powder samples, but not single crystals), the width of the elastic peak σ can be related to the mean kinetic energy $K_e(X)$ of atom X by

$$\sigma = \sqrt{\frac{4}{3}\overline{E_r^X}\,K_e(X)}, \quad (2)$$

where $\overline{E_r^X}$ is the mean recoil energy of element X: $q^2/2M_X$.[8] For targets consisting of atoms of different mass, the elastic peak consists of several components which for large enough q values will show up experimentally as separate peaks. It then becomes possible to determine the width of each peak and hence, the mean kinetic energy of each constituent.

Here, we use as targets SiO_2, $CaCO_3$, and Li_2CO_3. The measured kinetic energies obtained by electron scattering are compared with the results of two methods of calculations both based on the harmonic approximation: the first is the standard computational methods of infra-red (IR) spectroscopy[9] and the second relies on DFT.

C. Calculation of atomic kinetic energies

The atomic kinetic energy, K_e, of atoms constituting a molecular solid is contributed by three motions: external (lattice) translational-vibrations, librations (hindered rotations) of the whole molecule, and internal molecular vibrations. In ionic

This article is copyrighted as indicated in the article. Reuse of AIP content is subject to the terms at: http://scitation.aip.org/termsconditions. Downloaded to IP: 130.56.107.4 On: Mon, 02 Nov 2015 03:18:08

molecular solids, e.g., Li_2CO_3, the binding between the Li cation and the molecular CO_3 anionic unit is much weaker than the strong covalent bonds within the CO_3 anion. Thus, K_e of the O and C atoms in Li_2CO_3 is expected to be governed mainly by the internal vibrational frequencies of the anion. The present semi-empirical (SE) approach for calculating K_e utilizes the experimental internal and external characteristic frequencies measured by IR and Raman techniques and in some cases by inelastic neutron scattering (INS); this SE approach assumes the harmonic approximation and a decoupling between the three modes of motion.

The procedure of calculating the kinetic energy of the carbon and oxygen atoms constituting the CO_3 unit is applicable to both Li_2CO_3 and $CaCO_3$. Note that the carbonate anion has a trigonal symmetry (D_{3h}) forming a planar equilateral triangle with the O-atoms at the vertices and the C-atom at the center of mass; CO_3 has thus 6 normal internal modes, two of which are degenerate due to the symmetry of the molecule. Besides the internal vibrational modes, $K_e(X);(X = C, O)$ is also contributed by the external motions of translational- and librational-vibrations of the whole molecule. Thus, the kinetic energy of the X atom in CO_3 may be written as

$$K_e(\mathrm{X}) = S_t(\mathrm{X})\alpha(\nu_t, T) + S_r(\mathrm{X})\alpha(\nu_r, T) + \sum_{j=1}^{6} S_j(\mathrm{X})\alpha(\nu_j, T), \quad (3)$$

where $S_t(\mathrm{X})$, $S_r(\mathrm{X})$, and $S_j(\mathrm{X})$ are the energy fractions taken by the X-atom in the external motions of vibrations (translational) and libration, and in the internal j ($j = 1 \ldots 6$) normal vibrations, respectively (Table I). $\alpha(\nu_l, T)$, defined as

$$\alpha(\nu_l, T) = h\nu_l \left(\frac{1}{e^{h\nu_1/kT} - 1} + \frac{1}{2} \right), \quad (4)$$

is the kinetic energy of an harmonic oscillator of frequency ν_l ($l = t, r, j$), with t and r, the characteristic frequencies of the lattice vibrations and librations of CO_3 in $Li_2CO_3/CaCO_3$, k the Boltzmann constant, and T the thermodynamic temperature. Note also that the contribution of translation and libration to the kinetic energy may be also deduced from a knowledge of the Debye temperature of the molecular solid via its bulk specific heat.[9] The fraction of the translational motion, (e.g., $S_t = 16/60$ for O atoms), is directly obtained from the mass ratio of the O atom to that of CO_3. $S_r(\mathrm{X})$ is deduced classically by accounting for the moments of inertia as dictated by the geometry of free CO_3.[9] $S_j(X)$, the energy fraction shared by the X atom in the jth internal mode, may be deduced as explained in Ref. 9. The necessary input data for the determination of the $S_j(\mathrm{X})$ values are the 6 experimental IR vibrational frequencies of CO_3^{2-} in Li_2CO_3 and $CaCO_3$ taken from the literature (Table I) and the corresponding four force constants: K_1 (bending of the O–C–O angle), K_2 (C–O symmetric stretch), K_3 (C–O asymmetric stretch), and K_5 (restoring force which brings back the C–O to the CO_3 molecular plane).[9]

It should be emphasized that the above calculation was carried out by assuming *free* CO_3 and is also applicable to CO_3 bonded is a crystal. It turns out that there is a slight difference between the two cases reflecting itself in small changes in geometry and normal frequencies. The overall effect of the above changes on the values of $K_e(\mathrm{C})$ and $K_e(\mathrm{O})$ was calculated and found to be small and less than 1%, thus justifying the above procedure. Note that the above SE procedure cannot be used to calculate $K_e(\mathrm{Li})$ because of the absence of any optical information to describe the Li motion in the molecular crystal. This drawback was overcome by using the phonon density of states (DOS), as is done using the DFT method.

D. Calculations based on DFT

The determination of K_e based on DFT calculations was done for the cases of SiO_2 and Li_2CO_3. The structural, electronic, and phonon properties of the monoclinic Li_2CO_3 and of α-SiO_2 (quartz) were recently simulated using DFT.[12–14] Validation of the calculations was achieved by comparing the resulting bulk, thermodynamic, and elastic properties against available theoretical data and experimental measurements, where a good agreement was found. In both studies, the partial density of states (PDOS) of each constituent atom in a supercell of Li_2CO_3 and α-SiO_2 was simulated.

TABLE I. Experimental frequencies[10,11] and calculated kinetic energy fractions $S_l(\mathrm{X})$. The characteristic frequencies of translation and libration[11] were adopted for calculating K_e of both $CaCO_3$ and Li_2CO_3. AB, SB, SS, and AS denote asymmetric bend (degenerate), symmetric bend, symmetric stretch, and asymmetric stretch (degenerate), respectively, of CO_3. The last two rows indicate the total energy fractions shared by the atoms in the external and internal modes of motions. Note that for each atom, the sum over all energy fractions is unity.[9]

				Spectroscopy		DFT		
		ν	k	Li_2CO_3, $CaCO_3$		Li_2CO_3		
l	Mode	cm^{-1}	10^5 dyn/cm	$S_l(\mathrm{C})$	$S_l(\mathrm{O})$	$S_l(\mathrm{C})$	$S_l(\mathrm{O})$	$S_l(\mathrm{Li})$
t	Trans.	200		0.2002	0.2667	0.1765	0.5291	0.1544
r	Lib.	300		0	0.3333	0.0240	0.0796	0.8266
1, 2	AB	680	0.5944	0.0767	0.0855	0.0192	0.0997	0.0094
3	SB	879	0.7470	0.2666	0.0222	0.2617	0.0243	0.0007
4	SS	1065	5.5125	0	0.1111	0.0018	0.1104	0.0002
5, 6	AS	1415	1.7235	0.1899	0.0478	0.2487	0.0286	0.0008
		External		0.2	0.6	0.2	0.61	0.98
		Internal		0.8	0.4	0.8	0.39	0.02

This article is copyrighted as indicated in the article. Reuse of AIP content is subject to the terms at: http://scitation.aip.org/termsconditions. Downloaded to IP: 130.56.107.4 On: Mon, 02 Nov 2015 03:18:08

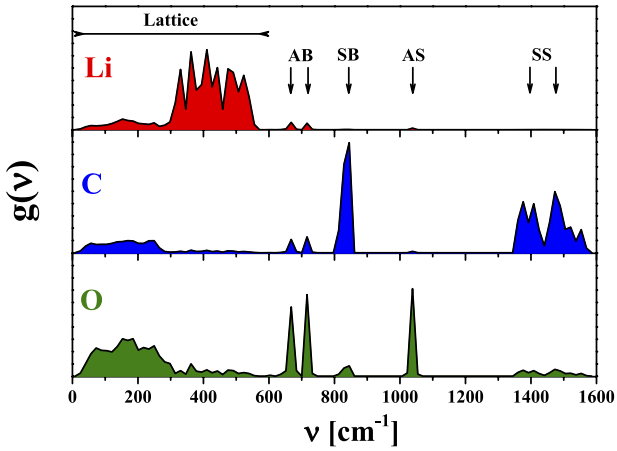

FIG. 1. $g_x(\nu)$ profiles for Li_2CO_3, as calculated using DFT in Refs. 12 and 13. Indicated in the upper plot are the lattice phonon spectral range (0-600 cm^{-1}) and the optical characteristic internal (normal) modes of the carbonate unit. AB, SB, SS, and AS correspond to the asymmetric bend (double degenerate), symmetric bend, symmetric stretch, and asymmetric stretch (double degenerate) of the carbonate unit.

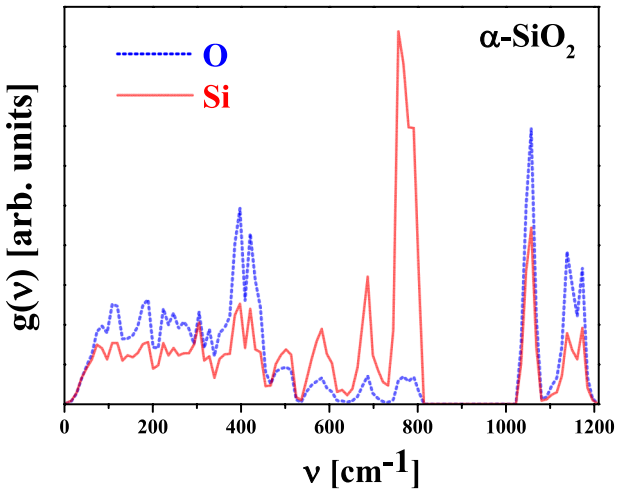

FIG. 2. $g_x(\nu)$ profiles (x = Si-solid, O-dashed) for SiO_2 (quartz), calculated and provided by the authors of Ref. 14.

The above calculated PDOS was utilized in the present study for deducing the mean kinetic energy, K_e, of the Li, C, and O atoms in Li_2CO_3 and of Si and O in SiO_2. In addition, in Ref. 13, the projection of the PDOS was also calculated along each of the three crystallographic directions enabling the kinetic energy of each constituent atom to be estimated along and perpendicular to the molecular plane of the carbonate unit. The PDOS of the X atom in the lattice supercell, hereby denoted as $g_x(\nu)$, provides the frequency distribution covering the entire range of lattice and internal phonon states. Figure 1 depicts the DFT calculated PDOS of the C, O, and Li atoms in Li_2CO_3, as an average over the calculated PDOS of Refs. 12 and 13, and Fig. 2 shows the calculated PDOS for SiO_2.

The figure emphasizes the fact that the Li atoms mostly participate in the (low-frequency) lattice modes and are only weakly affected by the internal, more energetic, modes of the carbonate unit. Fig. 1 also illustrates the fractions shared by the C and O atoms in the internal modes, in close correlation to the data calculated in Table I using the standard spectroscopic method.[9] Finally, it is interesting to note that despite of the optical normal modes being a single frequency features, while the phonon spectra give the actual continuous frequency distribution, both yield K_e(C) and K_e(O) values which are in close agreement (see Table I). For a crystal, $K_e(X)$ can be written as

$$K_e(X) = \frac{3}{2}\frac{\int_{\nu_i}^{\nu_f} g_X(\nu)\alpha(\nu)d\nu}{\int_{\nu_i}^{\nu_f} g_X(\nu)d\nu}, \quad (5)$$

with $\alpha(\nu_i)$ corresponding harmonic oscillator of the ith phonon state, and ν_i, ν_f the frequency boundaries of the $g_x(\nu)$. Table II summarizes the calculated kinetic energies of the atomic constituents of $CaCO_3$ and Li_2CO_3 using the above semi-empirical and DFT procedures.

It is clearly noted from Table II that for both carbonate salts, the ECS measurements and the two types of theoretical approaches systematically yield K_e(C) > K_e(O). At first glance, this outcome could be understood intuitively from the fact that the C-atom, being the light partner in the CO_3 unit, is expected to share the major part of the normal frequencies.

TABLE II. Calculated and ECS measured atomic kinetic energy of ^{16}O and ^{12}C and of the ^{7}Li, ^{28}Si, and ^{40}Ca cations in $CaCO_3$, Li_2CO_3, and SiO_2 at 295 K. DFT values were calculated using Eq. (5) where in Li_2CO_3 an average over raw data from Refs. 12 and 13 was taken. Raw data for SiO_2 were adapted from Ref. 14. Semi-empirical values were calculated from Eq. (3) using the lattice and internal frequencies of Table I. Experimental starred values are corrected for multiple scattering based on Monte Carlo simulations as discussed in Section IV B.

	Calculated (meV)					Experiment (meV)		
	Spectros.		DFT			ECS		
Sample	O	C	O	C	Cation	O	C	Cation
$CaCO_3$						69 ± 2	101 ± 3	48 ± 1
						64 ± 2*	94 ± 3*	46 ± 1*
Li_2CO_3	61.7	97.4	60.5	98	50.8	64 ± 2	100 ± 3	57 ± 5
						62 ± 2*	98 ± 3*	52 ± 5*
SiO_2	-	-	62.2	...	65.2	66 ± 3	...	70 ± 2
						61 ± 3*	...	68 ± 2*

This article is copyrighted as indicated in the article. Reuse of AIP content is subject to the terms at: http://scitation.aip.org/termsconditions. Downloaded to IP: 130.56.107.4 On: Mon, 02 Nov 2015 03:18:08

The geometry of the carbonate molecule, where the C atom is centered at the equilateral O_3 triangle, imposes however some restrictions on the mobility of the C atom. From an examination of the calculated energy fractions of Table II, one may clearly see that the C atom is excluded from both the symmetric stretch motion ($S_4 = 0$), having the strongest internal frequency, as well as from the external rotational modes ($S_r = 0$). Nonetheless, the energy fractions shared by the C atom in the remaining modes compensate for the above loss and the overall outcome is in favor of K_e(C) relative to K_e(O).

It is very interesting to note that the semi-empirical calculations produce practically the same results as those of the DFT method. It is also interesting to note that for the Li cations the DFT value of K_e(Li) is 50.8 meV (Table II). This is far higher than that of a pure Li metal which may be calculated by using the Debye approximation yielding K_e(Li) = 42.3 meV at 295 K obtained using a Debye temperature of θ (Li) = 448 K for metallic Li. Note that the value for metallic Li is only ≈11% larger than that of a free Li atom being $\frac{3}{2}kT$, whereas the value for Li cations is 35% larger, complying with the fact that the ionic bond between Li and CO_3 is far stronger than the metallic Li bond.

III. BAND GAP RESULTS

A. SiO_2

The first example we discuss is SiO_2. The SiO_2 layer was grown on a Si wafer by thermal oxidation and was 200 nm thick, much thicker than the probing depth of our electron scattering experiment (≈65 nm). Here, the band gap value is well established (8.9 eV[15]) and it is used here as a test case for the validity of the analysis method.

In the analysis procedure, we try to fit the elastic peak *plus* the onset of the inelastic part of the spectrum. The elastic peak fitting procedure is described extensively in Ref. 16. For homogeneous samples, the contribution of each element I_i is proportional to its concentration and its cross section for elastic scattering over 135° which has been tabulated.[17] Its intrinsic width is related to its kinetic energy.

These aspects are all evident in Fig. 3 for an experiment of a SiO_2 sample on which a small amount of Au (≈1 Å) was deposited. The incoming beam here, and for all spectra reported in this work, was along the surface normal. The first peak is due to the heaviest atom present: Au and the large intensity of this peak is due to its large cross section, which scales approximately as Z^2. The second and third peaks are due to Si and O. Both peaks are considerably wider than the Au peak, illustrating that the Doppler broadening is resolved. The Si and O peak area ratio reflects their cross section and the stoichiometry of the film (the fit indicates a Si:O concentration ratio is within 5% of the nominal stoichiometry). The Au layer was added to help establish the energy resolution of the spectrometer. Au has a low Debye temperature (170 K), and hence at room temperature its kinetic energy should be close to $\frac{3}{2}kT$. From the observed width and the calculated Doppler broadening, one can deduce the experimental resolution. Aided by this knowledge, one can then extract the Doppler

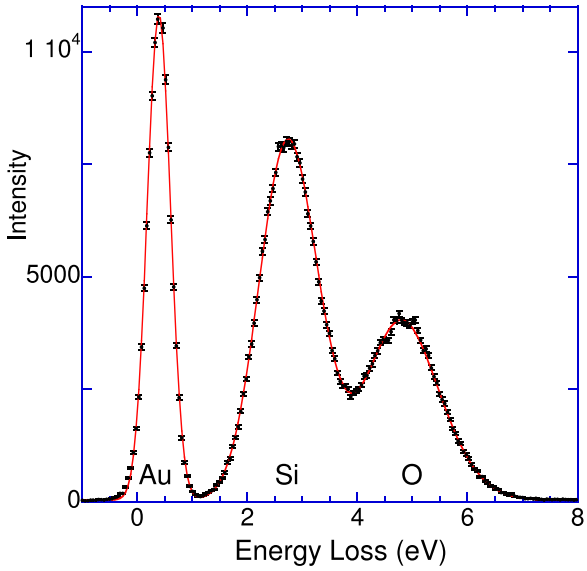

FIG. 3. The elastic peak of 40 keV electrons backscattered from SiO_2 on which ≈1 Å of Au was deposited.

broadening of the Si and O peak. The fit describes the data very well and the obtained values for the mean kinetic energy are given in Table II.

The onset of the energy loss spectrum was studied for a second sample, without Au deposition. Measurements were done at 5 keV (Fig. 4) and at 40 keV (Fig. 5). At 5 keV, there is still a noticeable asymmetry in the SiO_2 elastic peak. Compared to the 40 keV measurement, the recoil shifts are 8 fold smaller and not fully resolved any more but still influence the peak shape. The energy loss spectrum at 5 keV is very similar to the ones published by Jin *et al.*,[18] and the loss structure for the 40 keV measurement appears slightly more "washed out." At both energies, the elastic peaks can be fitted with the same kinetic energy and stoichiometry (and the tabulated cross section at 5 and 40 keV) and the Si and O components of the fit are shown as well.

The probability that an electron creates an electron-hole pair is taken to be independent of the atom that scattered the electron elastically. If the atom was stationary, its contribution to the inelastic part of the spectrum would start at $\overline{E_r^X} + E_{\text{gap}}$ and be proportional to $CI_X(E - E_{\text{gap}})^A$ with A, the assumed exponent of the onset. The onset is broadened by both the experimental resolution and the Doppler broadening (which depends on the element that scattered the electron elastically), as determined from the elastic peak. The results are shown in the lower panel of Figs. 4 and 5. As the onset is sharper at 5 keV, we will mainly use this measurement for the discussion of the band gap. The fit with an exponent $A = 1.5$ is marginally better in reproducing the shape of the onset of the energy loss spectra. The inferred gap values for the fit with $A = 0.5$ and $A = 1.5$ are quite different, ≈9.5 eV and ≈9.0 eV, respectively. This is due to the rapid onset for $A = 0.5$ and the more gradual onset for $A = 1.5$.

The obtained values are only meaningful if they do not depend on the cut-off energy of the fit. This is investigated in Table III. There is a strong correlation between C and E_{gap} values. The effect of a decrease in C can be compensated to

This article is copyrighted as indicated in the article. Reuse of AIP content is subject to the terms at: http://scitation.aip.org/termsconditions. Downloaded to IP: 130.56.107.4 On: Mon, 02 Nov 2015 03:18:08

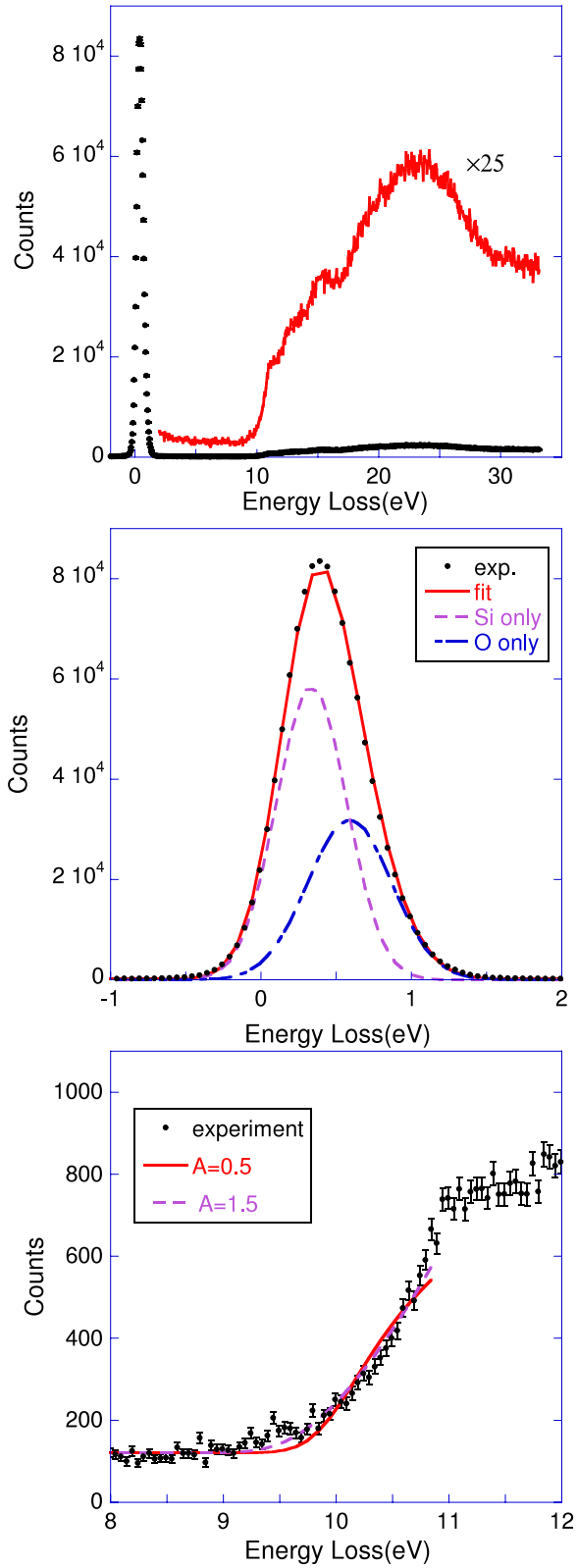

FIG. 4. Spectra taken at 5 keV from a SiO_2 sample over a wide energy range (top). The elastic peak is clearly asymmetric and can be fitted with a Si and an O component (center). The lower panel shows the onset of the inelastic contribution fitted with different exponents as described in the main text.

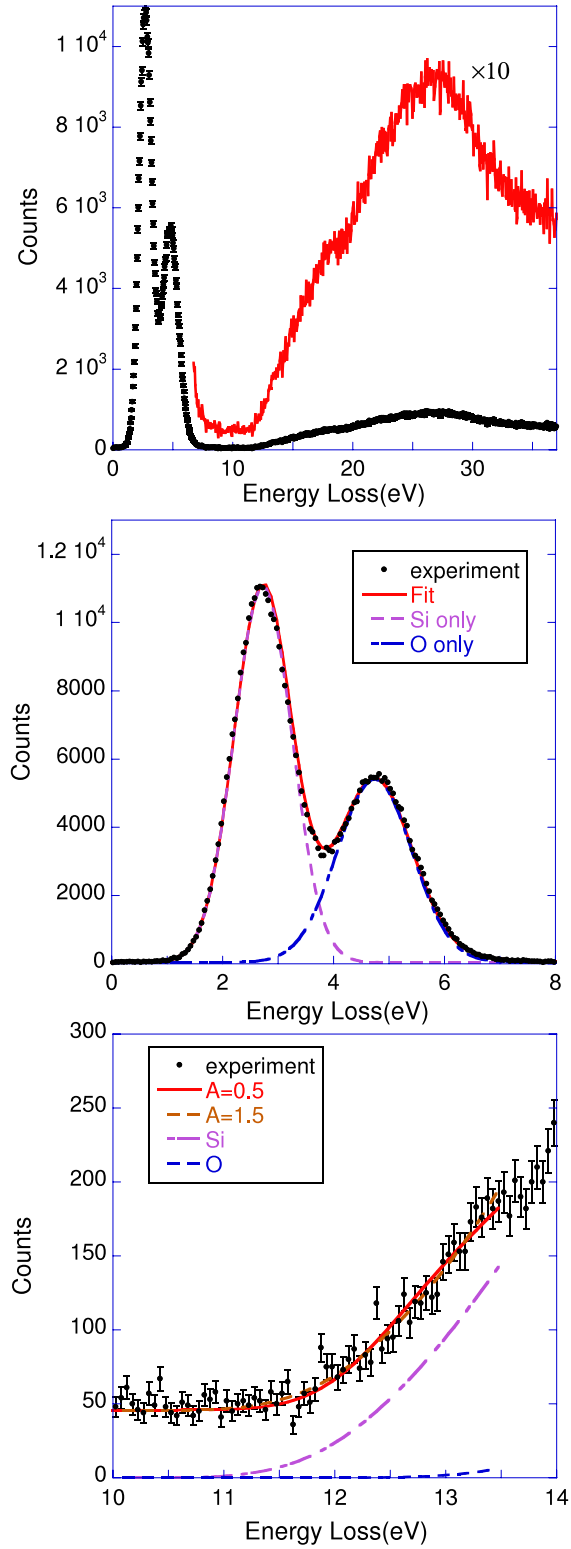

FIG. 5. Similar figure for Fig. 4 but now for an incoming energy of 40 keV. In the lower panel, we show now as well the contribution of electrons scattered from Si and O to the onset of the loss spectrum.

some extent by a decrease of E_{gap} and the values for which the best fit is obtained depend somewhat on the energy of the upper limit of the fit. For each cut-off energy, the E_{gap} value obtained is 0.5 eV smaller for $A = 0.5$ compared to $A = 1.5$. SiO_2 is an indirect gap insulator; hence, the approach of Ref. 2 suggests $A = 1.5$. The value for E_{gap} obtained with this exponent is 9 ± 0.2 and is indeed consistent with the commonly accepted value of 8.9 eV.

For the 40 keV measurement, one obtains an E_{gap} of 8.86 ± 0.1 using $A = 1.5$ and 9.55 ± 0.1 using $A = 0.5$. Thus,

This article is copyrighted as indicated in the article. Reuse of AIP content is subject to the terms at: http://scitation.aip.org/termsconditions. Downloaded to IP: 130.56.107.4 On: Mon, 02 Nov 2015 03:18:08

TABLE III. Influence of the upper limit of the fit for the 5 keV measurement on the obtained values for E_{gap} and C.

Fit limit	E_{Gap}, $A = 0.5$	C, $A = 0.5$	E_{Gap}, $A = 1.5$	C, $A = 1.5$
10.35	9.06 ± 0.1	0.0033	8.6 ± 0.3	0.0022
10.6	9.3 ± 0.1	0.0051	8.8 ± 0.2	0.0033
10.85	9.55 ± 0.08	0.0082	9.0 ± 0.1	0.0048
11.1	9.7 ± 0.06	0.010	9.1 ± 0.1	0.0056
11.35	9.65 ± 0.05	0.010	9.0 ± 0.1	0.0048

the analysis method gives very consistent values for the 5 keV and 40 keV measurements, which confirms the assumption that also the onset of the loss spectrum is affected by Doppler broadening.

B. $CaCO_3$

A second example that was studied was $CaCO_3$. Here, the information about the band gap is much more scarce. The usually quoted value of 6.0 eV was obtained from REELS data taken at lower energy (200 eV),[19] where the technique is very surface sensitive. The onset of the inelastic spectrum in that paper is not particularly sharp. DFT band structure calculations indicate that $CaCO_3$ is an indirect gap semiconductor with a band gap of ≈5 eV.[20–22]

Two samples were measured here: calcite single crystal and a pill pressed from $CaCO_3$ powder. The elastic peak was again studied at 40 keV after deposition of a small amount of Au. The obtained fit is shown in Fig. 6. The separation of the Au–Ca and Au–O was somewhat smaller than expected for 40 keV incoming energy. The incoming energy was treated as a fitting parameter, and turned out to be ≈38 keV. Thus, the sample surface charged by approximately 2 keV. From the fit, we obtained a nominal stoichiometry of $Ca_{1.0}C_{1.1}O_{3.0}$ using the tabulated cross sections. The larger error for C indicates that it is more difficult dealing with this element, as it appears at a shoulder only. The obtained values for the mean kinetic energy are also shown in Table II. They are consistent with earlier published data.[24] With the knowledge of the mean kinetic energy, we can analyze the 5 keV spectra of $CaCO_3$ (without Au) in the same way as was done for SiO_2. Two different samples were studied at 5 keV: a calcite crystal and a pill pressed from a powder. The results shown in Fig. 7 are for the pill. The energy loss spectrum is shown on a wide energy scale in the top panel. It is compared with a TEM-EELS energy loss spectrum of calcite from geological origin, taken from Ref. 23. The zero point of their spectrum (it did not contain the elastic peak) was slightly adjusted for better agreement. Most features are seen in both spectra, and the reduced intensity at larger losses in the TEM-EELS spectrum is a consequence of reduced multiple scattering in a thin sample. The elastic peak of the 5 keV data could again be fitted with the mean kinetic energy obtained at 40 keV (central panel), and the lower panel shows the onset of the contribution due to inelastic excitations. Two fits were done. Assuming a value $A = 1.5$, one obtains a band gap of 7.1 ± 0.2 eV. A value of 7.5 ± 0.2 was obtained for $A = 0.5$.

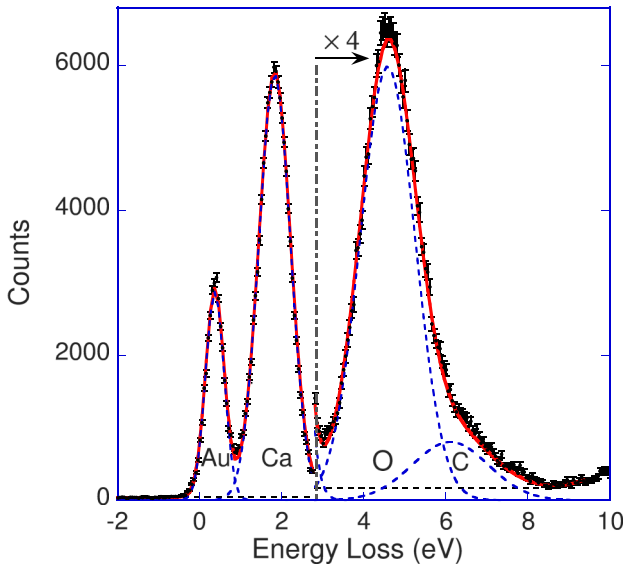

FIG. 6. 40 keV measurement of a $CaCO_3$ pill on which ≈1 Å of Au was deposited.

The calcite single crystal sample displayed strong charging. At 40 keV nominal incoming energy, the Ca–O separation was consistent with an incoming energy near 32-35 keV. Using the nominal value of the incoming energy of 5 keV, the calculated elastic peak shape was much broader than the observed one. Again, treating the incoming energy as a fitting parameter, it was inferred that the sample surface has charged by ≈2.5 keV. In Fig. 8, the onset of the band gap is compared for these two samples. The single crystal sample shows a somewhat more gradual onset of the loss spectrum. Using $A = 1.5$, a band gap is obtained here of 6.6 eV, about 0.5 eV less than for the pill material.

C. Li_2CO_3

Finally, we consider the case of Li_2CO_3. It plays an important role in the Li-air battery technology[25] and medical applications. DFT calculations give here a band gap of 4.9-5.1 eV,[12,13,26] whereas a GW calculation gives a value of 8.83 eV.[26] There are no experimental values of the band gap known to us. Here, we used again a pill pressed from a powder (Alfa Aesar 99.99%). Such powder is known to have the monoclinic structure.[27] Li_2CO_3 forms a hexagonal phase at high pressure[28] which has a rather different calculated band gap,[13] but this phase transforms back to the monoclinic one at ambient pressure.

For these very light materials, the recoil shifts are large and the onset of the band gap overlaps with the contribution of the lightest element present: Li. For Li, even the recoil shift for the two isotopes (^{6}Li and ^{7}Li) is noticeably different, and the contribution of each isotope was fitted separately. The concentration of ^{6}Li was determined by a mass spectrometer to be 7.5%. Au was again deposited on the surface, but now with a nominal thickness of only ≈0.2 Å. As the Au signal was easily separated from the Li_2CO_3 signal, even for 5 keV incoming energy, all the measurements were done with Au on the surface. The results for 3 different energies (5 keV, 25 keV, and 40 keV) are shown in Fig. 9. For the highest incoming energy, fitting of the spectrum becomes difficult as the onset of the inelastic

This article is copyrighted as indicated in the article. Reuse of AIP content is subject to the terms at: http://scitation.aip.org/termsconditions. Downloaded to IP: 130.56.107.4 On: Mon, 02 Nov 2015 03:18:08

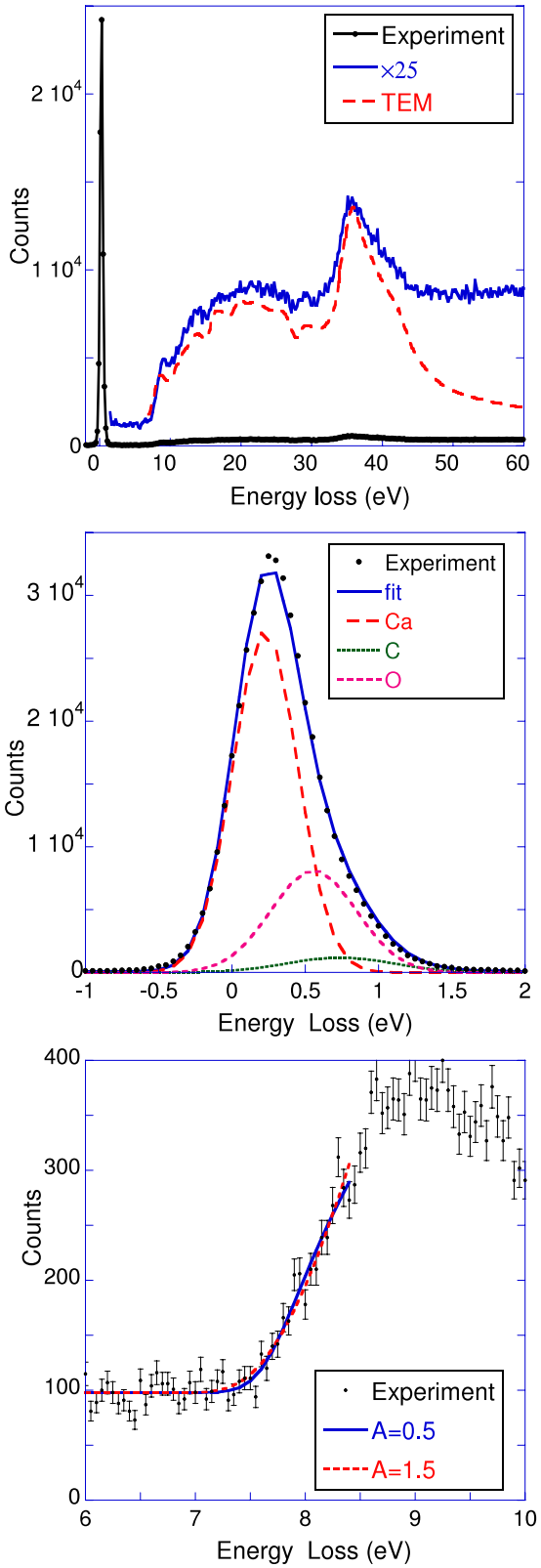

FIG. 7. Figure similar to Fig. 4 but now for $CaCO_3$. The dashed line in the upper panel, which is the loss spectrum obtained by TEM-EELS,[23] is shown for comparison.

spectrum extends under the Li peaks (especially for ^{6}Li), and determining the width (and area) of the Li contribution now depends critically on the shape of the background assumed. Hence, spectra taken at the 3 incoming energies were fitted in

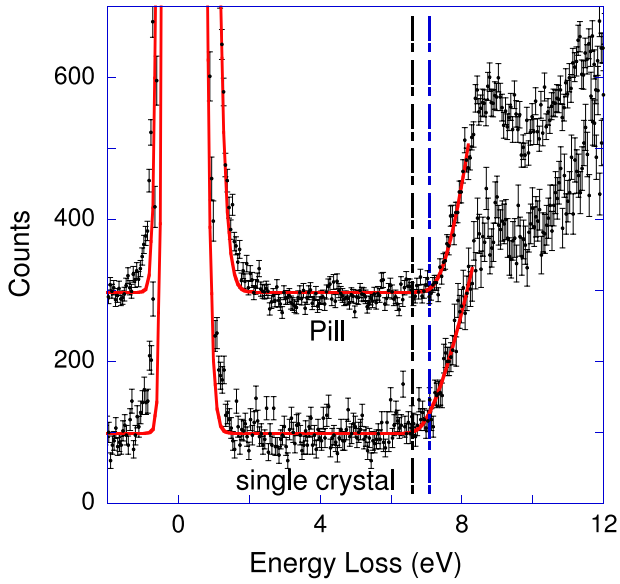

FIG. 8. A comparison of the 5 keV energy loss spectra for a calcite single crystal and calcite powder compressed in a pill.

such a way that the same band gap was used in all three cases as well as the same *A* value. The nominal stoichiometry derived from the fit was $Li_{2.0}C_{0.90}O_{3.0}$. Here, the errors are somewhat larger due to the weakness of the Li signal but still agrees

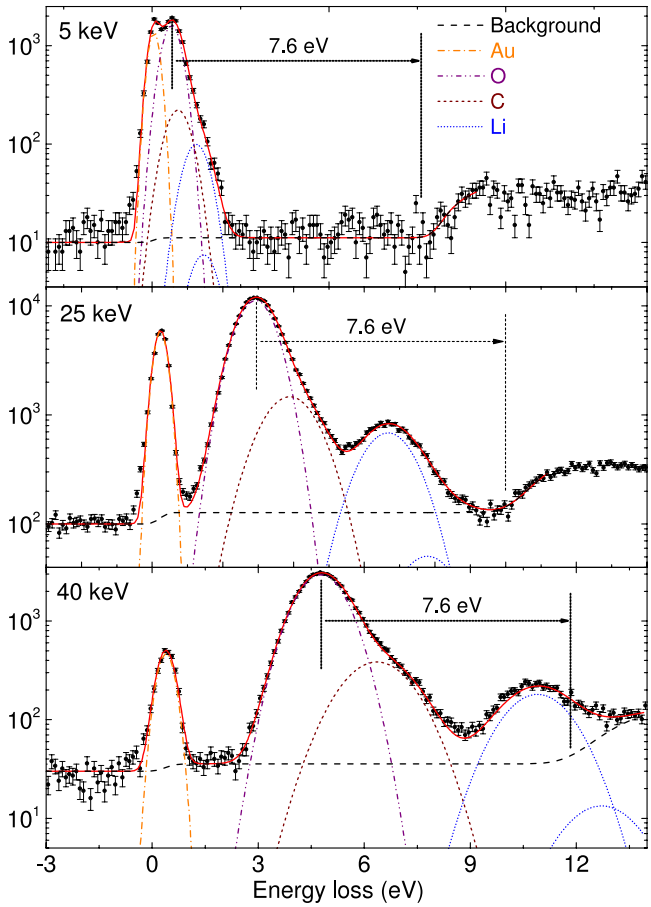

FIG. 9. Spectra of a Li_2CO_3 on which some Au was deposited, taken at 5 keV, 25 keV, and 40 keV incoming energy. The decomposition of the elastic peak in different components is shown as well.

This article is copyrighted as indicated in the article. Reuse of AIP content is subject to the terms at: http://scitation.aip.org/termsconditions. Downloaded to IP: 130.56.107.4 On: Mon, 02 Nov 2015 03:18:08

within 10% with the nominal composition. The Au atoms are at the surface and in the fitting procedure did not contribute to the onset seen, as electrons scattered from Au did not travel through Li_2CO_3. Li_2CO_3 is a direct gap semiconductor[13] and the plots in Fig. 9 are for $A = 0.5$.

The obtained band gap was 7.6 eV for $A = 0.5$ and 7.1 eV for $A = 1.5$. These values are larger than the DFT value, but smaller than the value obtained by a GW calculation.[26] Using this fitting procedure, we obtained a good fit assuming the nominal stoichiometry. The obtained kinetic energies are given in Table II as well. In this case, only a combined understanding of the band gap and the elastic peak shape leads to meaningful results.

IV. DISCUSSION

A. Bandgap measurement

The measurement of the band gap by REELS is conceptually very easy, but in reality it is quite hard to extract precise values. In this work, we extract band gap values based on a fitting procedure that describes the elastic peak precisely and an assumed energy dependence of the onset of the loss feature $I = C(E - E_{gap})^A$. Here, it is demonstrated that varying A from 0.5 to 1.5 changes the obtained band gap by about 0.5 eV. The procedure developed for TEM-EELS by Rafferty and Brown[2] seems to lead to the right band gap value for SiO_2 indicating that $A = 1.5$ could also be the right exponent for analysing REELS spectra for indirect gap semiconductors. For $CaCO_3$ compressed powder, we obtained significant larger values (7.15 ± 0.2 eV for $A = 1.5$ and 7.5 ± 0.2 eV for $A = 0.5$) than the value of 6 ± 0.35 eV reported by Baer and Blanchard.[19] For the single crystal calcite measurement, the band gap values are about 0.5 eV smaller, but still larger than those of Baer and Blanchard. For Li_2CO_3, the obtained gap is between 7.1 ($A = 1.5$) and 7.6 eV ($A = 0.5$), in between the DFT and GW values. Any claim of the extraction of precise (e.g., 0.1 eV precision) band gap value in a REELS experiment without knowledge of the functional shape of the onset of the loss intensity should be treated with caution.

B. Mean kinetic energy

In Table II, we have seen reasonable, but not perfect agreement between calculated and measured mean-kinetic energies. One of the crucial assumptions for the validity of the analysis here is occurrence of only one large-angle scattering event. This assumption was investigated using Monte Carlo simulations. In brief, electrons impinging along the surface normal are followed in the crystal. Trajectories are calculated based on the elastic scattering cross section as calculated by ELSEPA.[29] The electrons are followed until they leave the solid again, *or* their path length exceeds 10 times the inelastic mean free path λ, which is ≈64 nm for 40 keV electrons in SiO_2.[30] If the electron leaves the crystal at an angle corresponding to the direction towards the detector, then the trajectory is "accepted," and the elastic peak is constructed based on these trajectories only.

For each deflection, the recoil losses are calculated in two different ways: (a) By assuming the scattering atom is stationary and the recoil energy is then simply $q^2/2M$. In this way, it is easy to pinpoint the influence of multiple elastic scattering events. (b) Assuming the atoms are vibrating, i.e., including the Doppler broadening. The momentum component of the scattering atom along $\boldsymbol{q}$ (p_q) is then assumed to be Gaussian with a width given by Eq. (2). For each collision, the momentum component p_q is chosen randomly from this Gaussian distribution and the recoil energy loss is calculated from Eq. (1). The contribution of these trajectories to the elastic peak will depend on the path length L. Only the fraction $\exp(-L/\lambda)$ of these trajectories will not create electronic excitations and thus contribute to the elastic peak. The simulated elastic peak is obtained from the sum of the detected trajectories, weighted by this factor.

Examples are shown in Fig. 10. Without Doppler broadening, there are two completely separated peaks in the recoil distribution, for scattering from Si and O. For the case of only a single elastic deflection, these peaks have a rectangular shape. This is due to the finite opening angle assumed. Unfortunately, it is too time consuming to perform these simulations for the actual opening angle of the experiment (≈0.2°). We carried out the simulations for opening angles between 3° and 12°. Only for opening angles of 12° does it contribute noticeable to the extracted mean kinetic energy. An opening angle of 3° was used in the final simulation.

For the trajectories with more than one deflection, the energy distribution does not have a rectangular shape, but is slightly broadened. In almost all these cases, the trajectory consists of one large angle scattering event and one or more small scattering angles. This is due to the shape of the elastic scattering distribution which is very strongly peaked for small scattering angles. Trajectories with many scattering events tend to be longer, and hence their contribution to the elastic peak decreases rapidly with increasing number of deflections.

In the bottom panel of Fig. 10, we show the simulated spectrum (dots) for one of more deflections as obtained when the Doppler broadening is taken into account. This spectrum is still quite noisy. It differs from the experimental one as no finite energy resolution is taken into account. Convoluting the obtained distribution with the experimental energy resolution (here, 0.37 eV FWHM), one obtains the smooth curve. Indeed this curve resembles the experiment very closely.

The smooth curve is then fitted in the same way as the experimental data are fitted, that is, we interpret the result of the simulations, assuming that only one elastic deflection took place. Good fits are obtained but the kinetic energy is slightly larger (≈2-3 meV for Si and ≈5 meV for O) than what is used as input to the simulations. This difference is due to multiple scattering. Correcting the experimentally obtained values by this difference we obtain 61 meV for O and 68 meV for Si, very close to the theoretical estimates.

Similar small corrections were obtained for Li_2CO_3 and $CaCO_3$ based on the same approach. It appears that the multiple scattering correction is the largest for the lightest element in a compound. For the lightest element, a relative small deflection from the heavy element (a frequent occurrence due to its

This article is copyrighted as indicated in the article. Reuse of AIP content is subject to the terms at: http://scitation.aip.org/termsconditions. Downloaded to IP: 130.56.107.4 On: Mon, 02 Nov 2015 03:18:08

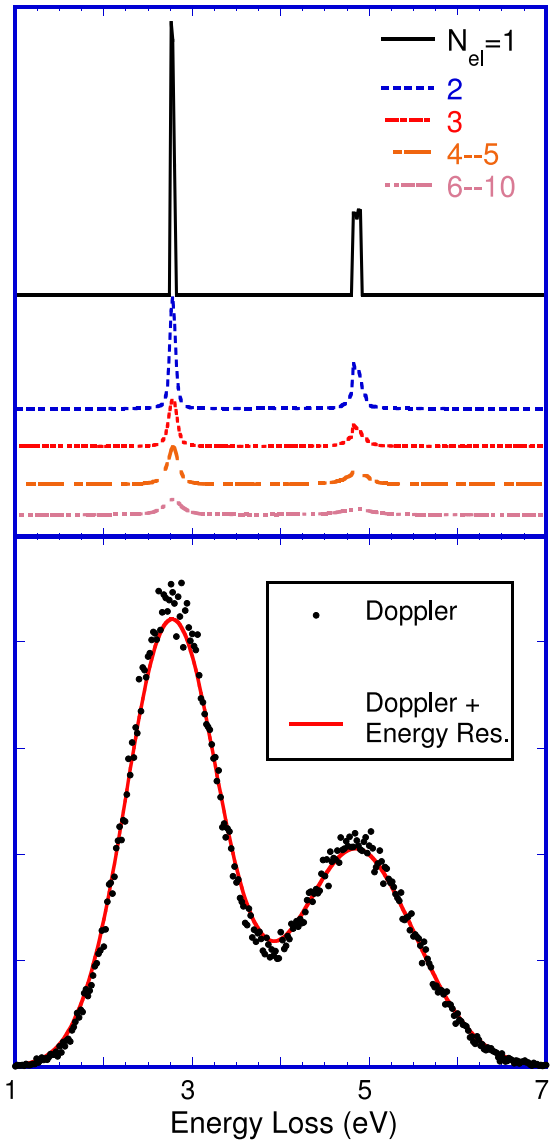

FIG. 10. In the top panel, we show for SiO_2 the distribution of the recoil energy for trajectories with the number of elastic collisions N_{el} as indicated. In this case, the scattering was assumed from stationary atoms. The lower panel (dots) shows the elastic peak of all trajectories, as obtained when the motion of the atom is taken into account. Applying the experimental energy resolution of 0.37 eV full-width half-maximum results in the smooth curve.

large elastic scattering cross section) in combination with a large-angle deflection from the light element (a relatively rare occurrence) has a significant contribution to the overall intensity and results in a broadening of the peak of the lightest element. In case of Li_2CO_3, it was hard to get enough statistics in the (weak) Li peak, and the obtained correction was from a simulation that ran over a 10 day period.

Thus, in summary, v-shaped trajectories dominate, else the spectrum would not separate in different peaks, each corresponding to a specific atom. Multiple deflections cause deviations from a perfect v-shape, but in almost all cases there is still one dominant collision over an angle close to the one dictated by the experimental setup (i.e., 135°). The simulations suggest that small deviations around this value cause some additional broadening and hence it has to be accounted for if one wants to extract mean kinetic energies with high accuracy. Similar conclusions on multiple scattering were obtained in the case of carbon in graphite and diamond.[31]

V. CONCLUSION

Clearly, these measurements contain information about the band gap and the mean kinetic energy of the atoms. Extracting accurate numbers for these quantities requires great care. For the precise determination of the mean kinetic energy, one cannot neglect the influence of multiple scattering. If this is done, the agreement between theory and experiment is quite good. For the determination of the band gap, a good understanding of the elastic peak shape is required. Moreover, the assumption made for the energy dependence of the onset of the loss spectrum has a significant influence on the value of the band gap obtained, and this assumption has to be justified on theoretical grounds. The technique, as described here, can have important applications for the determination of the band gap in thin films with thicknesses of several tens of nm, as under these conditions optical techniques are not easily applicable.

ACKNOWLEDGMENTS

We would like to thank Dr. Shun-Li Shang and Dr. Yuhua Duan for helpful correspondence concerning the DFT calculations and for providing the raw data used to plot Figure 1. We are grateful to Dr. Yevgeni Zakon from the geological survey of Israel (GSI) for measuring the isotopic abundance of lithium in the Li_2CO_3 powder. This work is made possible by a grant of the Australian Research Council. G.G.M. acknowledges support from CNPq: Conselho Nacional de Desenvolvimento Científico e Tecnológico—Brazil.

[1]B. L. French and S. W. King, J. Mater. Res. **28**, 2771 (2013).
[2]B. Rafferty and L. M. Brown, Phys. Rev. B **58**, 10326 (1998).
[3]M. Inokuti, Rev. Mod. Phys. **43**, 297 (1971).
[4]L. Gu, V. Srot, W. Sigle, C. Koch, P. van Aken, F. Scholz, S. Thapa, C. Kirchner, M. Jetter, and M. Rühle, Phys. Rev. B **75**, 195214 (2007).
[5]J. Park, S. Heo, J.-G. Chung, H. Kim, H. Lee, K. Kim, and G.-S. Park, Ultramicroscopy **109**, 1183 (2009).
[6]S. Schamm and G. Zanchi, Ultramicroscopy **96**, 559 (2003).
[7]M. Vos, Phys. Rev. A **65**, 12703 (2001).
[8]M. Vos, R. Moreh, and K. Tőkési, J. Chem. Phys. **135**, 024504 (2011).
[9]R. Moreh, O. Shahal, and V. Volterra, Nucl. Phys. A **262**, 221 (1976).
[10]G. Herzberg, *Infrared and Raman Spectra of Polyatomic Molecules*, Molecular Spectra Infrared and Raman Spectra and Molecular Structure Vol. 2 (Van Nostrand Reinold, New York, 1945).
[11]C. Carteret, M. De La Pierre, M. Dossot, F. Pascale, A. Erba, and R. Dovesi, J. Chem. Phys. **138**, 014201 (2013).
[12]S.-L. Shang, L. G. Hector, S. Shi, Y. Qi, Y. Wang, and Z.-K. Liu, Acta Mater. **60**, 5204 (2012).
[13]Y. Duan and D. C. Sorescu, Phys. Rev. B **79**, 014301 (2009).
[14]Y. Duan, H. Pfeiffer, B. Li, I. C. Romero-Ibarra, D. C. Sorescu, D. R. Luebke, and J. W. Halley, Phys. Chem. Chem. Phys. **15**, 13538 (2013).
[15]R. B. Laughlin, Phys. Rev. B **22**, 3021 (1980).
[16]G. Marmitt, L. Rosa, S. Nandi, and M. Vos, J. Electron Spectrosc. Relat. Phenom. **202**, 26 (2015).
[17]A. Jablonski, F. Salvat, and C. Powell, *NIST Electron Elastic Scattering Cross-Section Databases Version 3.2 SRD64* (National Institute of Standards and Technology, Gaithersburg MD, 2010).
[18]H. Jin, H. Shinotsuka, H. Yoshikawa, H. Iwai, S. Tanuma, and S. Tougaard, J. Appl. Phys. **107**, 083709 (2010).

This article is copyrighted as indicated in the article. Reuse of AIP content is subject to the terms at: http://scitation.aip.org/termsconditions. Downloaded to IP: 130.56.107.4 On: Mon, 02 Nov 2015 03:18:08

[19]D. Baer and D. L. Blanchard, Appl. Surf. Sci. **72**, 295 (1993).
[20]A. Skinner, J. LaFemina, and H. Jansen, Am. Mineral. **79**, 205 (1994).
[21]F. M. Hossain, G. E. Murch, I. V. Belova, and B. D. Turner, Solid State Commun. **149**, 1201 (2009).
[22]M. Brik, Phys. B **406**, 1004 (2011).
[23]K. S. Katti, M. Qian, D. W. Frech, and M. Sarikaya, Microsc. Microanal. **5**, 358 (1999).
[24]M. Vos, K. Tokesi, and I. Benko, Microsc. Microanal. **19**, 576 (2013).
[25]B. D. McCloskey, A. Speidel, R. Scheffler, D. C. Miller, V. Viswanathan, J. S. Hummelshoj, J. K. Norskov, and A. C. Luntz, J. Phys. Chem. Lett. **3**, 997 (2012).
[26]P. Albertus, G. Girishkumar, B. McCloskey, R. S. Sánchez-Carrera, B. Kozinsky, J. Christensen, and A. C. Luntz, J. Electrochem. Soc. **158**, A343 (2011).
[27]P. Pasierb, R. Gajerski, S. Komornicki, and M. Rekas, J. Therm. Anal. Calorim. **65**, 457 (2001).
[28]R. Grzechnik, P. Bouvier, and L. Farina, J. Solid State Chem. **173**, 13 (2003).
[29]F. Salvat, A. Jablonski, and C. J. Powell, Comput. Phys. Commun. **165**, 157 (2005).
[30]S. Tanuma, C. J. Powell, and D. R. Penn, Surf. Interface Anal. **21**, 165 (1994).
[31]M. Vos, R. P. McEachran, G. Cooper, and A. P. Hitchcock, Phys. Rev. A **83**, 022707 (2011).

This article is copyrighted as indicated in the article. Reuse of AIP content is subject to the terms at: http://scitation.aip.org/termsconditions. Downloaded to IP: 130.56.107.4 On: Mon, 02 Nov 2015 03:18:08